Evolution of $E2$ strength in the rare-earth isotopes ^{174,176,178,180}Hf

J. Wiederhold,[1,*] V. Werner,[1,2] R. Kern,[1] N. Pietralla,[1] D. Bucurescu,[3] R. Carroll,[4] N. Cooper,[2,†] T. Daniel,[4,‡] D. Filipescu,[3] N. Florea,[3] R-B. Gerst,[5] D. Ghita,[3] L. Gurgi,[4] J. Jolie,[5] R. S. Ilieva,[2,4] R. Lica,[3] N. Marginean,[3] R. Marginean,[3] C. Mihai,[3] I. O. Mitu,[3] F. Naqvi,[2] C. Nita,[3] M. Rudigier,[4,5] S. Stegemann,[5,§] S. Pascu,[3] and P. H. Regan[4,6]

[1]*Institut für Kernphysik Technische Universität Darmstadt, Schlossgartenstr. 9 64289 Darmstadt, Germany*

[2]*Wright Nuclear Structure Laboratory, Yale University, New Haven, CT 06520, USA*

[3]*"Horia Hulubei" National Institute for Physics and Nuclear Engineering, 077125, Bucharest-Magurele, Romania*

[4]*Department of Physics, University of Surrey, Guildford, Surrey GU2 7XH, United Kingdom*

[5]*Institut für Kernphysik Universität zu Köln, D-50937 Köln, Germany*

[6]*National Physical Laboratory, Teddington, Middlesex TW11 0LW, United Kingdom*

(Received 15 November 2018; revised manuscript received 15 January 2019; published 21 February 2019)

Mean lifetimes of yrast states of the isotopes ^{174,176,178,180}Hf have been measured using fast-electronic scintillation timing. Excited states of ^{174,176,178}Hf were populated via β decay, while ^{180}Hf was populated via Coulomb excitation. The lifetimes of the 2_1^+ and 4_1^+ states of all isotopes and the lifetimes of the 6_1^+ states of ^{174,178}Hf were measured, using the slope and the centroid shift methods. The mean lifetime, $\tau(4_1^+) = 85(13)$ ps, of ^{178}Hf has been determined for the first time. In addition, the mean lifetimes of the 2_1^- and the 3_1^- states of ^{176}Hf have been determined. Systematic uncertainties on the evolution of data as a function of neutron number were reduced by using the same setup for all the isotopes of interest. The data are in agreement with other recent lifetime measurements where available and shows a shift of the maximum of collectivity for the Hf isotopic chain from neutron midshell at $N = 104$ to $N = 100$.

DOI: 10.1103/PhysRevC.99.024316

I. INTRODUCTION

An important observable regarding the shape of even-even nuclei is the $E2$ transition strength from the ground state (gs) to the first 2^+ state, which is a measure of nuclear quadrupole collectivity. Along an isotopic chain a gradual evolution of the $B(E2; 2_1^+ \rightarrow 0_{gs}^+)$ is expected. Well-deformed nuclei, e.g., nuclei in the rare-earth region around the mass number $A \approx 170$, with a large quadrupole deformation, i.e., β deformation values of about 0.2–0.4 [1–14], typically exhibit large $B(E2)$ values in the order of 100 W.u. or more, while close to magic numbers single-particle excitations predominate and the $B(E2)$ strength is at a minimum (≈1–10 W.u.). In a naive valence-shell picture the $E2$ transition strength should increase toward, and maximize at midshell, increasing with the number of valence nucleons (holes). The expected maximum of collectivity at midshell can also be shown in the SU(3) limit of the interacting boson model [15,16].

It was pointed out by Zhang *et al.* [17], based on the available experimental data at that time, that $B(E2)$ values and g factors [18,19] of the first excited states of even-even nuclei around $A = 170$ do not maximize but instead saturate near midshell, as can be seen in Figs. 1(a) and 1(b). This has been explained qualitatively by an overlap of the proton and neutron wave functions and a reduction of the proton-neutron interaction strength near midshell. Furthermore, it was pointed out in Refs. [16,20] that the evolution of $E2$ strengths of the tungsten and hafnium isotopes exhibits an irregularity, which can be clearly identified in the differential of $B(E2)$ values defined as $\delta B(E2) = B(E2)_N - B(E2)_{N-2}$. A smooth trend of the differential is observed for heavier isotopes (osmium to lead), but oscillations or sharp drops were seen for the data on hafnium and tungsten isotopic chains. These oscillations may hint at nuclear structural anomalies or may simply point to incorrect experimental data (since the same $B(E2)_N$ value occurs in $\delta B(E2)_N$ and $\delta B(E2)_{N+2}$ [16]). Missing data and large uncertainties of experimental data provide motivation for new experiments in this region of the nuclear chart to clarify the situation [16,21–24], and indeed, discrepancies from literature values of the lifetime of the first excited 2^+ states of the hafnium and tungsten isotopes in the order of up to 20% were found. $B(E2)$ observables directly relate to the β degree of freedom. As such an effective β value is obtained from $\beta^2 \propto B(E2; 0_1^+ \rightarrow 2_1^+)$, and the $B_{4/2} = B(E2; 4_1^+ \rightarrow 2_1^+)/B(E2; 2_1^+ \rightarrow 0_{gs}^+)$ ratio quantifies the softness of the nuclear potential in β [25–27]. Unfortunately, data on the $B(E2; 4_1^+ \rightarrow 2_1^+)$ value were missing for ^{178}Hf, which complicates the analysis of the evolution of quadrupole collectivity in the isotopes under investigation.

In the current work, we present $E2$ transition strengths of the yrast bands of the isotopes ^{174,176,178,180}Hf extracted from

*jwiederhold@ikp.tu-darmstadt.de

†Present address: University of Notre Dame, Notre Dame, IN 46556, USA.

‡Present address: Department of Physics, Faculty of Science, Benue State University, PMB 102119, Makurdi, Nigeria.

§Present address: Institute for Nuclear and Radiation Physics, KU Leuven, 3001 Leuven, Belgium.

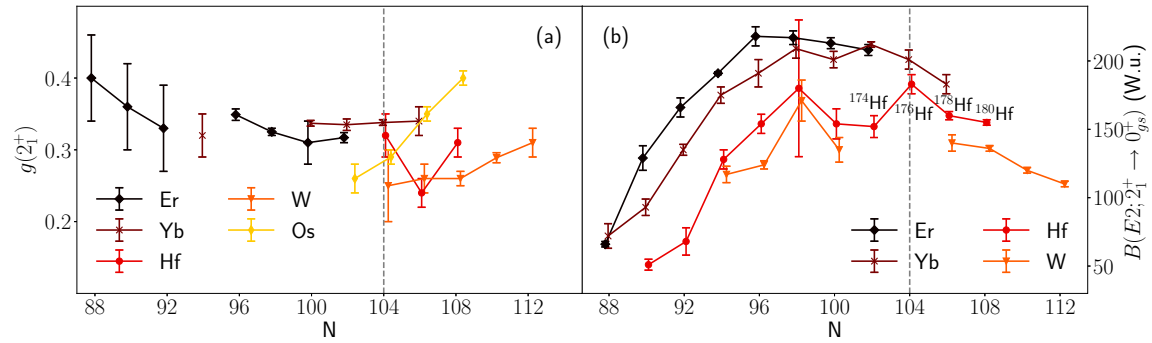

FIG. 1. (a) Systematics of g factors of first excited 2_1^+ states of even-even nuclei around neutron number $N = 104$ (marked with gray dashed line) of Er, Yb, Hf, W, and Os isotopes. The g factor values seem to saturate around (or slightly below) $N = 104$ apart from the Hf isotopic chain, which only has three data points. Data have been taken from Ref. [19]. (b) Systematics of $B(E2; 2_1^+ \rightarrow 0_{gs}^+)$ values of even-even Er, Yb, Hf, W, and Os isotopes around neutron number $N = 104$ (marked with vertical gray dashed line) from literature data [1–14,28]. The values of different isotopes are slightly shifted for a better visibility.

a measurement campaign, using fast electronic scintillation timing (FEST) at the IFIN-HH in Bucharest. Systematic uncertainties on their evolution across this sequence of nuclide were reduced by using the same setup for all isotopes of interest. Moreover, mean lifetimes of the nonyrast states (3_1^- and 2_1^- states of ^{176}Hf) have been determined and will be presented.

II. EXPERIMENT AND ANALYSIS

Excited states of ^{180}Hf were populated via Coulomb excitation induced by an ^{16}O primary beam at 55 MeV, just at the Cline-criterion for safe Coulomb excitation [29] and well below the Coulomb barrier at 88 MeV. The oxygen beam, delivered by the Bucharest FN Tandem accelerator, impinged on a 12-mg/cm^2-thick ^{180}Hf target. The enrichment of the target was 93.9% of ^{180}Hf with small contaminations from other stable Hf isotopes: ^{179}Hf(1.6%), ^{178}Hf(2.8%), ^{177}Hf(1.3%), and 0.4% of other isotopes. The other Hf isotopes ^{174,176,178}Hf were excited via β decay following the fusion-evaporation reactions ^{171}Yb(^{6}Li, 3n)^{174}Ta, ^{172}Yb(^{7}Li, 3n)^{176}Ta, and ^{174}Yb(^{7}Li, 3n)^{178}Ta at a beam energy of 30 MeV with target thicknesses of ^{172}Yb, 2.3 mg/cm^2; ^{171}Yb, 3 mg/cm^2; and ^{174}Yb, 2.5 mg/cm^2. The beam was cycled between ON (1 h) and OFF (1 h) to take in- and off-beam data. De-excitation γ rays were detected using the ROSPHERE detector array [30] in a configuration with 11 $LaBr_3$ and 14 HPGe detectors. The $LaBr_3$ and HPGe detectors were arranged in five rings around the target chamber.

The master-trigger condition for the experiment was set on either two or more coincident γ rays in the $LaBr_3$ detectors or two or more coincident γ rays in the HPGe detectors. In addition, for the ^{180}Hf data, for 2 h the trigger conditions were set to HPGe singles in order to be able to perform a Coulomb-excitation analysis of ^{180}Hf. The energy and the efficiency calibrations in the range between 121 keV and 1408 keV were done using a ^{152}Eu source, which was also used to determine the energy-dependent time walk of the experimental setup.

The lifetime of an excited nuclear state can be extracted using the fast-timing method by measuring the time difference between two signals coming from a populating and a depopulating transition. A detailed description can be found in Refs. [31–33]. The measured time difference Δt_m between two signals contains not only the effective lifetime τ_{eff}, i.e., the sum of the lifetimes that lie between the γ-ray transitions, but also the energy-dependent time walk [31]:

$$\Delta t_m = \tau_{\text{eff}} + t_{\text{tw},1}(E_{\gamma,1}) + t_{\text{tw},2}(E_{\gamma,2}). \quad (1)$$

To determine the lifetime, the energy-dependent time walk of each detector was determined using an ^{152}Eu source with its well-known γ lines from the γ decay of ^{152}Gd and ^{152}Sm ranging from 244 to 1299 keV, as described in Refs. [33–35], by fitting a polynomial function to the time response using the full energy peaks of the europium source. After applying the corrections the data wwere sorted into E_{γ,LaBr_3}-E_{γ,LaBr_3}-Δt cubes. Time-difference spectra between two transitions were extracted from these cubes by selecting the coincidence areas of the transitions (e.g., populating and depopulating transition of the nuclear state of interest) in the energy-energy plane (see Fig. 2). To exclude contaminants of other transitions on the time-difference spectrum, the $LaBr_3$ gates were compared with $E_{\gamma,\text{Ge}}$-$E_{\gamma,\text{Ge}}$ matrices and only pairs of coincidences, where a clean selection was guaranteed, were used. The resulting time difference was corrected for random coincidences and the Compton background below the full energy peaks in the energy spectrum (see also Fig. 3). This was done by selecting an area around the two-dimensional (2D) peak in the energy-energy plane.

The resulting delayed time distribution $D_\lambda(t)$, without any background contributions, is a convoluted function of the prompt response of the detection system $P(t')$ and the exponential decay of the nuclear state of interest [36]:

$$D_\lambda(t) = n\lambda \int_{-\infty}^{t} P(t')e^{-\lambda(t-t')}dt', \quad (2)$$

with the transition rate $\lambda = 1/\tau$ and the normalization n. If the lifetime of the nuclear state of interest is larger than the full width at half maximum (FWHM) of the system's response, a simple fit of the exponential decay of the time distribution gives the lifetime of the nuclear state. In the case where the lifetime is small in comparison to the FWHM of the system's response other methods, e.g., the centroid shift

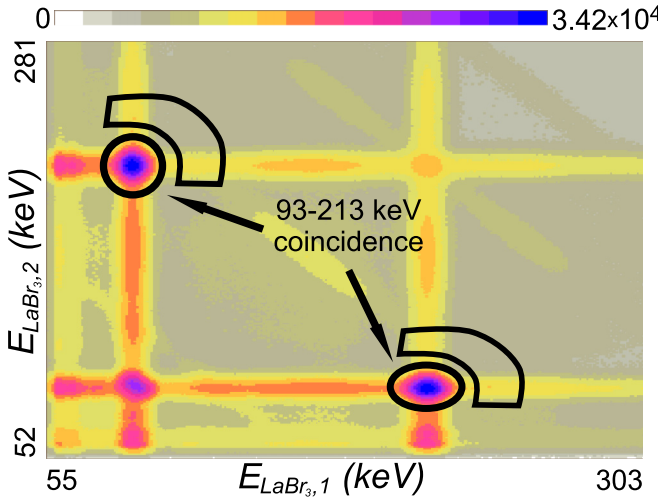

FIG. 2. Section of the $E_{\gamma,\mathrm{LaBr_3}}$-$E_{\gamma,\mathrm{LaBr_3}}$ matrix obtained after projection of the $E_{\gamma,\mathrm{LaBr_3}}$-$E_{\gamma,\mathrm{LaBr_3}}$-$\Delta t$ cube. Marked are the coincidence areas of the γ-ray pair 93 and 213 keV, corresponding to the transitions $2_1^+ \rightarrow 0_{gs}^+$ and $4_1^+ \rightarrow 2_1^+$ of ^{178}Hf. They are not distinguishable from the γ-ray pair $8_1^- \rightarrow 8_1^+$ (88 keV) and $4_1^+ \rightarrow 2_1^+$ (213 keV) as mentioned in the text.

method [31,32], have to be used to determine the lifetime of the nuclear state. The centroid of the time distribution is defined as [37]:

$$C(D_\lambda) = \langle t \rangle = \frac{\int t D_\lambda(t) dt}{\int D_\lambda(t) dt}, \tag{3}$$

resulting, for the delayed case (start condition on the feeding transition), in

$$\tau = C_d(D_\lambda) - C_d(P), \tag{4}$$

with the centroid of the delayed time distribution $C_d(D_\lambda)$ and of the system's prompt response $C_d(P)$. When the gates are switched also $C(D)$ and $C(P)$ switch places in the equation. After the time-walk correction $C_d(P)$ is equal to the centroid $C_a(P)$ of the antidelayed time distribution. It follows for the centroid difference [38]:

$$\Delta C = C_d(D) - C_a(D), \tag{5}$$

$$= C_d(P) + \tau - (C_a(P) - \tau), \tag{6}$$

$$= 2\tau. \tag{7}$$

Lifetimes of the long-lived 2_1^+ states of ^{174,176,178,180}Hf and of the 2_1^- state of ^{176}Hf, in the range of ns, were determined using the slope method using γ-γ coincidences within the $LaBr_3$ detectors. Energy gates were set on the $4_1^+ \rightarrow 2_1^+$ and $2_1^+ \rightarrow 0_{gs}^+$ transitions in the case of the 2_1^+ state and on the $2_2^- \rightarrow 2_1^-$ and $2_1^- \rightarrow 2_1^+$ transitions for the 2_1^- state. The most reliable region for the fit was determined by moving time gates with different widths across the time-difference spectrum. Only the regions without fluctuations, i.e., contributions from the prompt peak or the background, were used for the fits. The time-difference spectra, including the fits, are shown in Figs. 4 and 7(a).

The lifetimes of short-lived excited states, in this work 4_1^+, 6_1^+, 3_1^- states, were determined by the centroid shift method. Figures 5 and 7(b) show the delayed and antidelayed time distributions for the short-lived yrast states of ^{174,176,178,180}Hf

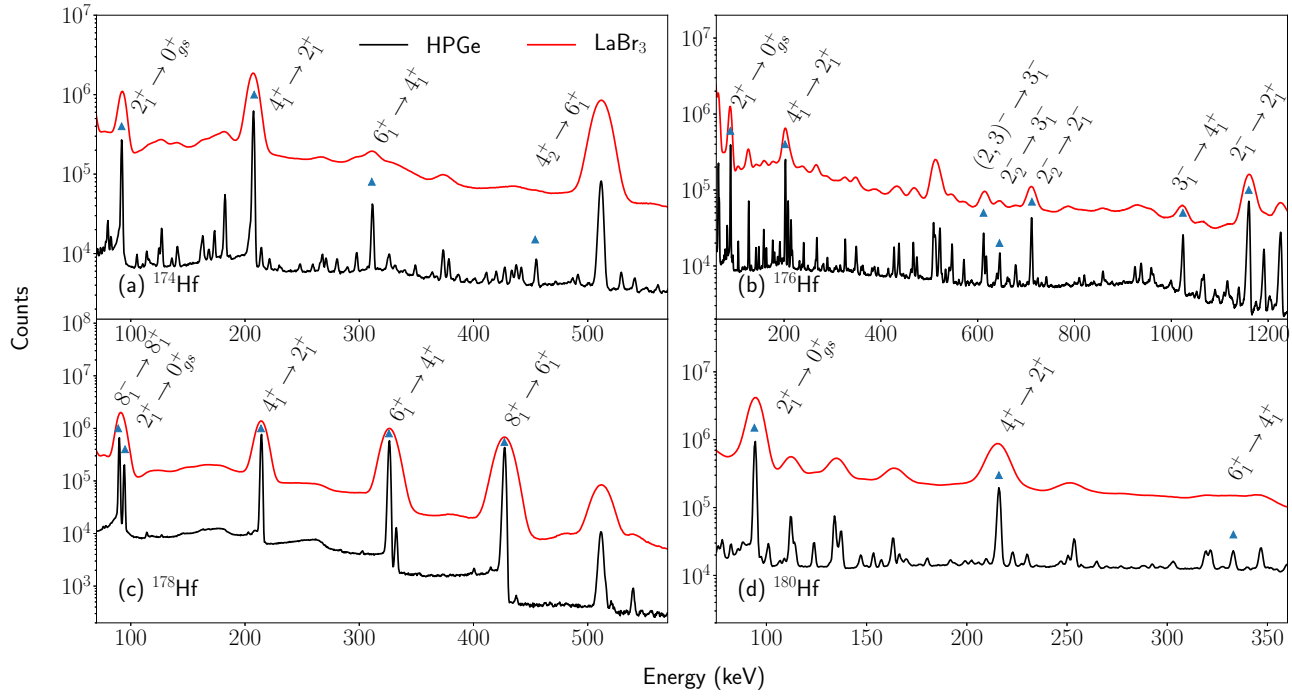

FIG. 3. Partial energy spectra of all $LaBr_3$ (red) and HPGe detectors (black) for (a) ^{174}Hf, (b) ^{176}Hf, (c) ^{178}Hf, and (d) ^{180}Hf. Transitions used for the determination of the lifetimes are denoted by blue triangles.

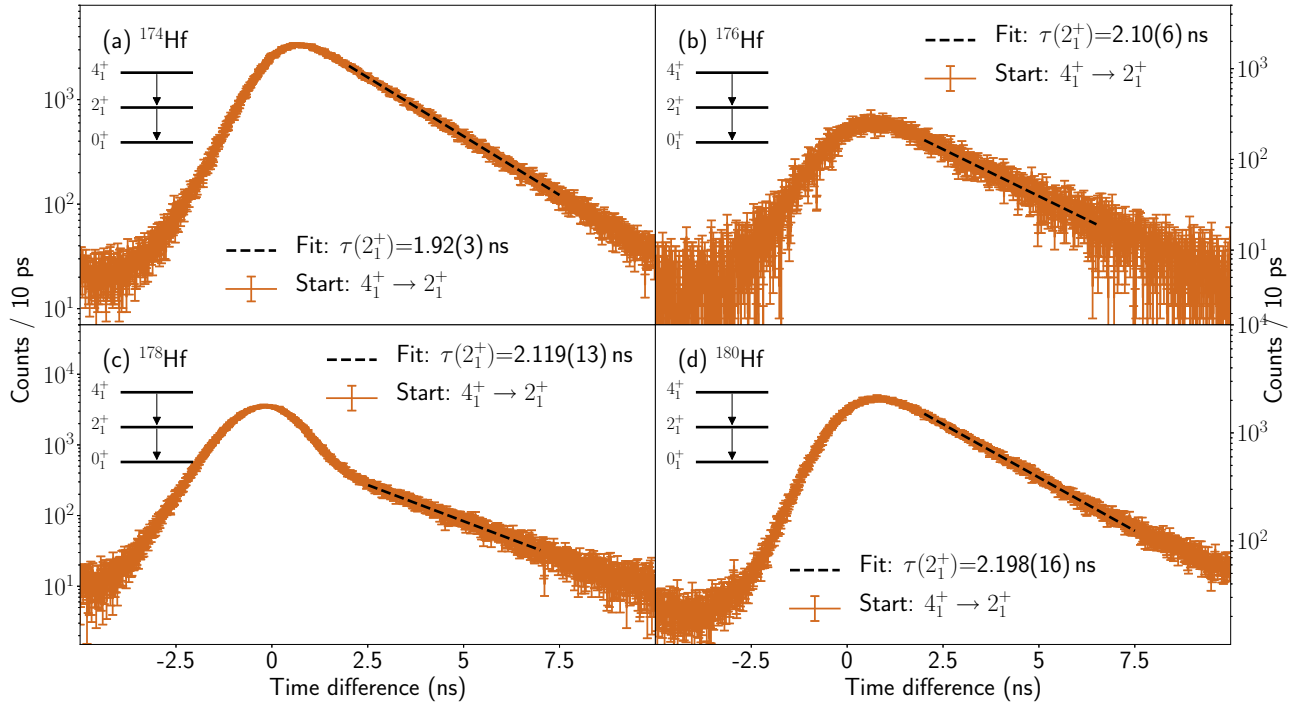

FIG. 4. Logarithmic plots of the time-difference spectra for the decays of 2_1^+ states of the isotopes ^{174,176,178,180}Hf from (a)–(d). Final linear fits are indicated by the dashed black lines.

and for $\tau(3_1^-)$ of ^{176}Hf. The used decay cascades are shown next to the time distributions. In the case of ^{176}Hf, smaller gate widths were taken because of the higher transition density [see Fig. 3(b)], resulting in lower statistics of the time distributions and therefore larger uncertainties of the determined lifetimes.

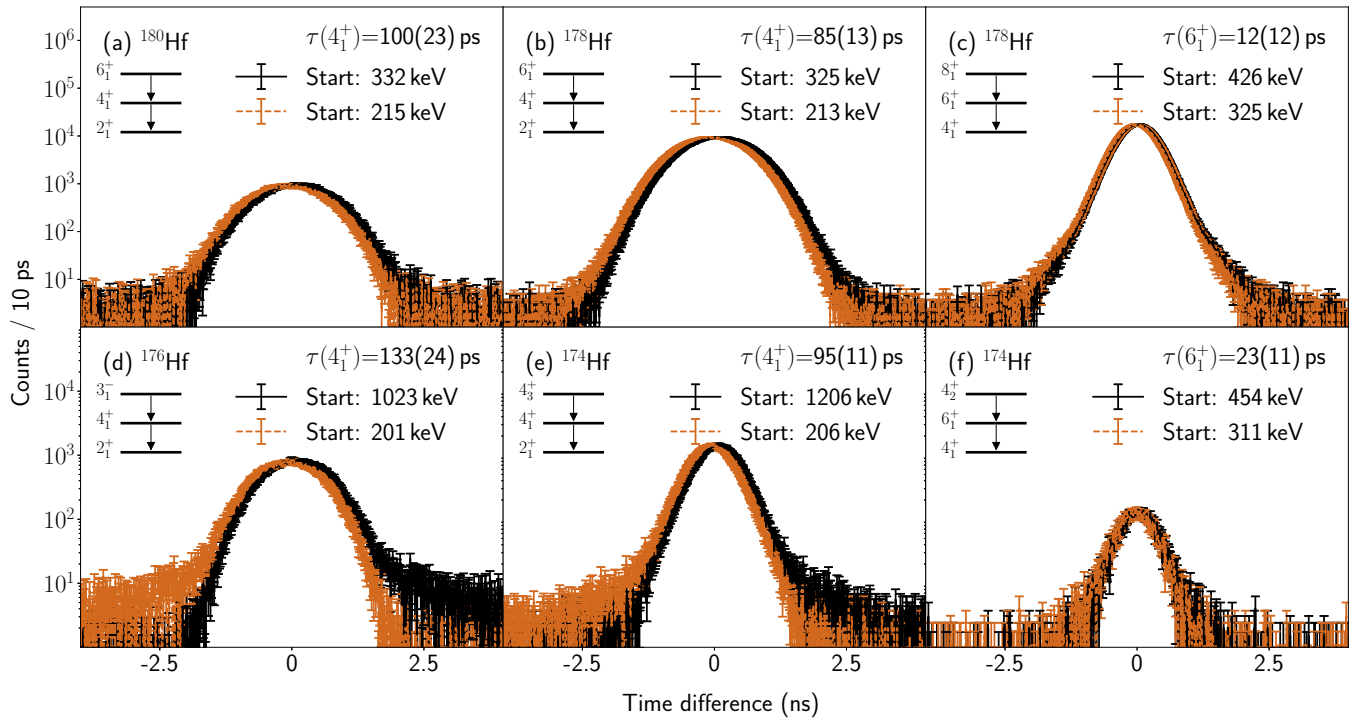

FIG. 5. Logarithmic plots of the time-difference spectra for the decays of short lived (range of ps) yrast states of the isotopes ^{180,178,176,174}Hf. The delayed time spectra are shown in black (solid lines) and the antidelayed spectra in orange (dashed lines). (a) The time-difference spectra for the $6_1^+ \rightarrow 4_1^+ \rightarrow 2_1^+$ cascade of ^{180}Hf, (b) for the $6_1^+ \rightarrow 4_1^+ \rightarrow 2_1^+$ cascade of ^{178}Hf, (c) for the $8_1^+ \rightarrow 6_1^+ \rightarrow 4_1^+$ cascade of ^{178}Hf, (d) for the $3_1^- \rightarrow 4_1^+ \rightarrow 2_1^+$ cascade of ^{176}Hf, (e) for the $4_3^+ \rightarrow 4_1^+ \rightarrow 2_1^+$ cascade of ^{174}Hf, and (f) for the $4_2^+ \rightarrow 6_1^+ \rightarrow 4_1^+$ cascade of ^{174}Hf.

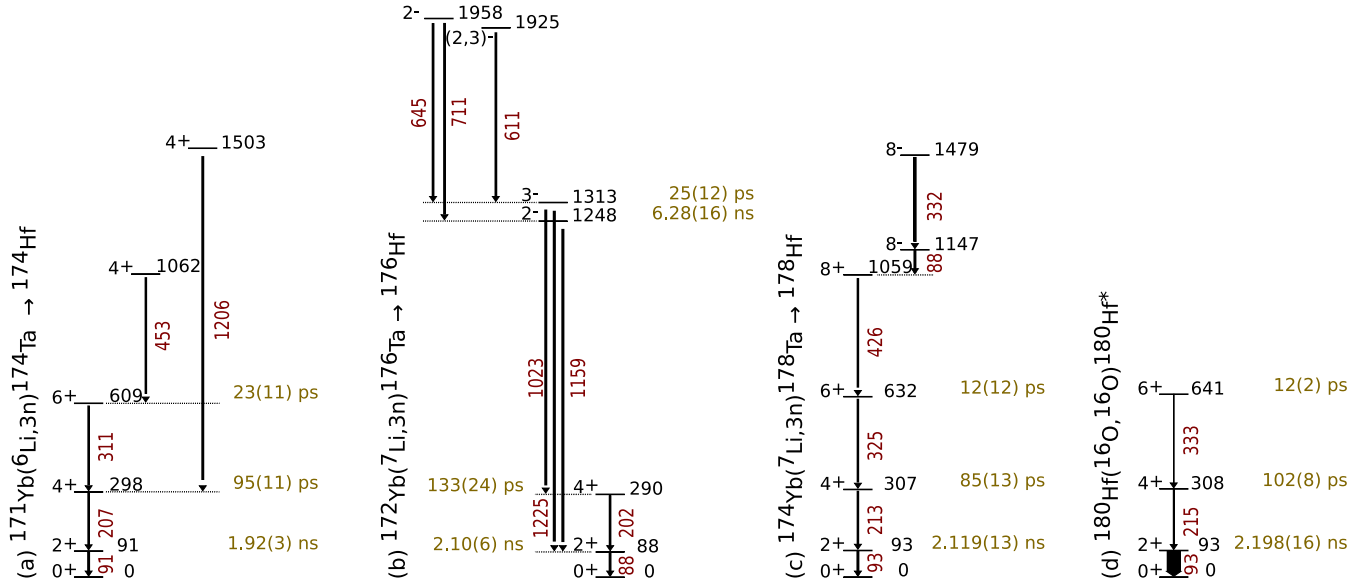

FIG. 6. Partial level schemes of the investigated Hf isotopes, $^{174-180}$Hf (a)–(d). Shown are the states and transitions used for fast-timing lifetime measurement. The determined mean lifetimes are given in yellow. In the case of ^{180}Hf, the transition widths correspond to the observed γ-ray intensity.

III. RESULTS

A. ^{174}Hf

Figure 3 shows the obtained γ-ray spectra of the HPGe and $LaBr_3$ detectors. Transitions relevant for the determination of the investigated lifetimes are marked with triangles.

The decay of ^{174}Ta to ^{174}Hf via electron capture populates excited positive-parity states [39]. The yrast band is populated up to the 6_1^+ state and transitions feeding and depopulating these states can be identified in the energy spectrum [see Fig. 3(a)]. The partial level scheme of ^{174}Hf, including the investigated states, is depicted in Fig. 6(a). Lifetimes of the 2_1^+, 4_1^+, and 6_1^+ states were extracted from the data. The pair of $6_1^+ \rightarrow 4_1^+$ and $4_1^+ \rightarrow 2_1^+$ coincident transitions has not been used for the determination of the lifetime of the 4_1^+ state as for the other investigated isotopes, because the sum energy of both transitions $[E(6_1^+ \rightarrow 4_1^+) + E(4_1^+ \rightarrow 2_1^+) = 517$ keV] is close to 511 keV. As a result, Compton-scattered events from 511-keV annihilation γ rays contaminate the coincidence area of the $6_1^+ \rightarrow 4_1^+$ and $4_1^+ \rightarrow 2_1^+$ transitions. Hence, the pair of the $4_3^+ \rightarrow 4_1^+$ and $4_1^+ \rightarrow 2_1^+$ transitions has been used instead to determine the lifetime of the 4_1^+ state. The obtained results are given in Table I.

B. ^{176}Hf

The decay of ^{176}Ta to ^{176}Hf via electron capture results in a complicated decay scheme with many transitions [41,42], in comparison to the decay of ^{178}Hf, as can be seen from Fig. 3(b). The part of the level scheme relevant for this work is shown in Fig. 6(b). Apart from the yrast band, also a low-lying negative-parity $K = 2$ band of ^{176}Hf is strongly populated via this decay. The mean lifetimes of the 2_1^- state and for the first time of the 3_1^- state have been determined (see Fig. 7). For the determination of $\tau(3_1^-)$ two possible populating transitions have been used, i.e., the transitions at 611 keV $[(2, 3)^- \rightarrow 3_1^-]$ and at 645 keV $(2_2^- \rightarrow 3_1^-)$, resulting in a more precise value of $\tau(3_1^-) = 25(12)$ ps. The extracted mean lifetime of the 2_1^- state is lower than the adopted value given in Ref. [11] but in agreement with other measurements, e.g., Ref. [43].

Since many transitions can be seen, the gates for the determination of the mean lifetimes have to be carefully selected in the $LaBr_3$ detectors. All selected energy gates were cross checked within the energy spectra of the HPGe detectors. Table I summarizes the extracted mean lifetimes of ^{176}Hf.

C. ^{178}Hf

Excited states of ^{178}Hf were populated via β decay from ^{178}Ta. Primarily, the 8^- isomeric state at an energy of 1147 keV was populated, which decays through the emission of γ rays through the yrast band. The obtained γ-ray spectrum is shown in Fig. 3(c). The decay transition of the 8_1^- state to the 8_1^+ state (88.9 keV) and the transition $2_1^+ \rightarrow 0_{gs}^+$ (93.2 keV) are very close in energy. For this reason, these transitions cannot be distinguished within the $LaBr_3$ detectors [see Fig. 3(c)] and it is not possible to set additional energy gates in the HPGe detectors since both transitions are from the same decay cascade. Selecting the region marked in Fig. 2 results in a time-difference spectrum which is a superposition of two time-difference distributions, on one hand a distribution gated on the $2_1^+ \rightarrow 0_{gs}^+$ and $4_1^+ \rightarrow 2_1^+$ transitions and on the other hand a distribution gated on the $8_1^- \rightarrow 8_1^+$ and $4_1^+ \rightarrow 2_1^+$ transitions. The latter corresponds to the effective mean lifetime of the 4_1^+, 6_1^+, and the 8_1^+ states combined (all on the order of ps). However, the time-difference distribution is a superposition of a delayed and an antidelayed distribution, since the ordering of the gates is reversed for the two cases [the 88 keV transition is above the 213-keV transition and

TABLE I. Measured mean lifetimes of excited states of ^{174,176,178,180}Hf. Adopted literature values were taken from Refs. [10–13] and from Ref. [24]. Values obtained from the Coulomb-excitation analysis are indicated with CLX. Newly obtained lifetimes and transition strengths are marked by an asterisk*. Two different cascades can be used to determine $\tau(3_1^-)$ of ^{176}Hf, resulting in an adopted value of $\tau(3_1^-) = 25(12)$ ps. Weighted average value of $\tau(2_1^+)$, $\tau(4_1^+)$, and $\tau(6_1^+)$ of ^{174,176}Hf have been taken from Ref. [24] and this work. $\tau_{\text{weighted}}(4_1^+)$ of ^{180}Hf has been taken from the CLX calculation and the fast-timing measurement. $B(E2;\lambda \to \lambda - 2)$ have been determined from τ_{weighted} and $\tau_{\text{exp.}}$ with the internal conversion coefficients taken from BrIccFO [40].

Isotopes	J_n^p	Gate-1	Gate-2	$\tau_{\text{exp.}}$ (ps)	$\tau_{\text{lit.}}$ (ps)	τ_{weighted} (ps)	α [40]	$B(E2)$ (W.u.)
^{174}Hf	2_1^+	$4_1^+ \to 2_1^+$	$2_1^+ \to 0_1^+$	1920(30)	1847(58) [24]	1905(30)	5.12(8)	194(4)
	4_1^+	$4_3^+ \to 4_1^+$	$4_1^+ \to 2_1^+$	95(11)	111(7) [24]	106(7)	0.258(4)	282(16)
	6_1^+	$4_2^+ \to 6_1^+$	$6_1^+ \to 4_1^+$	23(11)	23(7) [24]	23(6)	0.071(1)	198^{+69}_{-41}
^{176}Hf	2_1^+	$4_1^+ \to 2_1^+$	$2_1^+ \to 0_1^+$	2100(60)	2121(87) [24]	2107(49)	5.77(9)	181(5)
	4_1^+	$3_1^- \to 4_1^+$	$4_1^+ \to 2_1^+$	133(24)	130(9) [24]	130(8)	0.279(4)	250(16)
	2_1^-	$2_2^- \to 2_1^-$	$2_1^- \to 2_1^+$	6280(160)	6720(250) [11]	6407(200)	–	–
	3_1^-	$2_2^- \to 3_1^-$	$3_1^- \to 4_1^+$	26(18)*	–	25(12)*	–	–
	3_1^-	$(2,3)^- \to 3_1^-$	$3_1^- \to 4_1^+$	25(16)*	–		–	–
^{178}Hf	2_1^+	$4_1^+ \to 2_1^+$	$2_1^+ \to 0_1^+$	2119(13)	2155(33) [12]	2124(12)	4.66(7)	163(3)
	4_1^+	$6_1^+ \to 4_1^+$	$4_1^+ \to 2_1^+$	85(13)*	–	85(13)*	0.232(4)	296^{+53*}_{-39}
	6_1^+	$8_1^+ \to 6_1^+$	$6_1^+ \to 4_1^+$	12(12)	16(1) [12]	16(1)	0.062(1)	221(14)
^{180}Hf	2_1^+	$4_1^+ \to 2_1^+$	$2_1^+ \to 0_1^+$	2198(16)	2191(14) [13]	2194(11)	4.63(7)	155(2)
	4_1^+	$6_1^+ \to 4_1^+$	$4_1^+ \to 2_1^+$	100(23)	102(14) [13]	102(11)	0.225(4)	234^{+28}_{-23}
	4_1^+	CLX		103(12)				
	6_1^+			12(2)	14(1) [13]	14(1)	0.059(1)	225(16)

the 93-keV transition is below 213 keV, cf. Fig. 6(c)]. Due to the fact that the tail, stemming from the effective mean lifetime of the 4_1^+, 6_1^+, and the 8_1^+ states, is located on the other side of the time difference distribution, it is possible to identify the exponential decay of the long-lived 2_1^+ state and to extract its mean lifetime [see Fig. 4(c)]. In addition to $\tau(2_1^+)$ the mean lifetimes of the 4_1^+ (for the first time) and 6_1^+ states have been determined by using the centroid-shift method. The results are presented in Table I.

D. ^{180}Hf

Mean lifetimes of ^{180}Hf have been determined via FEST and Coulomb excitation, with the computer code CLX [44], based on the original code by Winther and De Boer [45]. Since the ^{180}Hf target had been also used in a previous fusion-evaporation experiment, there was still activated material in the target and many transitions from other isotopes, e.g., ^{181}Ta, ^{182}W, and ^{184}W can be identified in the HPGe energy spectrum [see Fig. 3(d)]. Moreover, for a determination of the mean lifetime of the first 2^+ state the contribution from the ^{178}Hf content of the target has to be taken into account. The transition energies of the $2_1^+ \to 0_{\text{gs}}^+$ and $4_1^+ \to 2_1^+$ transitions are very close in energy (93.2 keV vs. 93.3 keV and 213.4 keV vs. 215.3 keV) in ^{178}Hf and ^{180}Hf. They cannot be separated in the $LaBr_3$ detectors, resulting in a superposition in the time-difference spectrum. However, with the measured mean lifetimes of ^{178}Hf and the observed intensity of the $6_1^+ \to 4_1^+$ transition of ^{178}Hf at 332 keV, the ^{178}Hf content can be subtracted. The determined mean lifetimes together with the transitions used are listed in Table I. In addition to the mean lifetimes determined by the fast-timing measurement

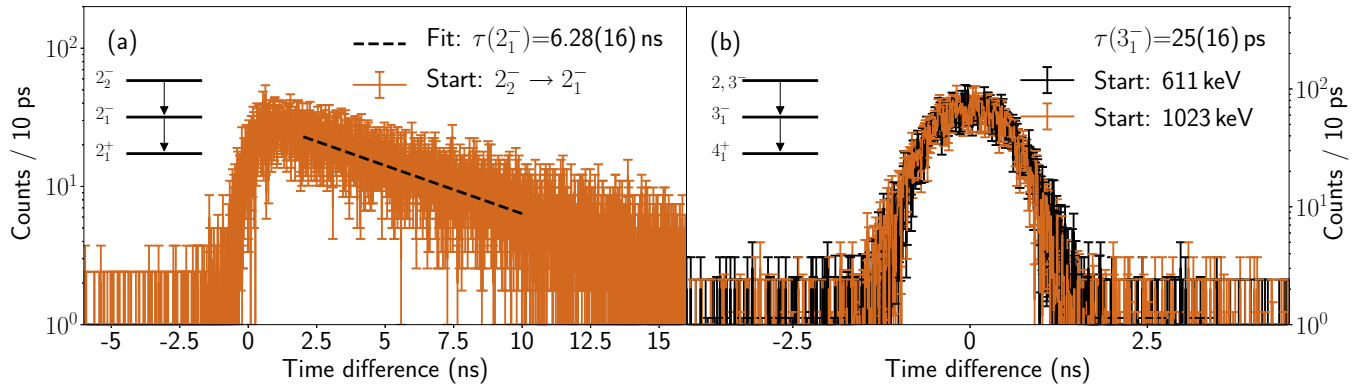

FIG. 7. (a) Logarithmic plots of the time-difference spectrum for the decay of 2_1^- state of the isotopes ^{176}Hf. Final linear fit is indicated by the dashed black line. (b) Delayed (black) and antidelayed (orange) time distributions of the cascade $(2/3)^- \to 3_1^- \to 4_1^+$.

the values obtained by the Coulomb-excitation analysis are shown.

The Coulomb-excitation yields were calculated from the efficiency-corrected γ-ray intensities, with the ^{178}Hf γ-ray transition intensities subtracted, normalized to the $2_1^+ \rightarrow 0_{gs}^+$ transition. The yields of the excited states, relative to that of the 2_1^+ state, are proportional to the relative Coulomb-excitation cross sections. The matrix elements of the $4_1^+ \rightarrow 2_1^+$ and $6_1^+ \rightarrow 4_1^+$ transitions were fitted to reproduce the relative Coulomb-excitation yields with the multiple Coulomb-excitation code CLX [44]. The energy loss of 18 MeV of the beam in the target was taken into account. Uncertainties for the Coulomb-excitation analysis were determined via variation of the matrix elements within the range of the calculated Coulomb-excitation yields. Both values of $\tau(4_1^+)$ agree within their uncertainties and a weighted average of these independent evaluations can be extracted: $\tau(4_1^+) = 102(11)$ ps.

The determined mean lifetimes are directly related to the transition strength

$$\frac{1}{\tau} = 8\pi \frac{\lambda+1}{\lambda[(2\lambda+1)!!]^2} \left(\frac{E_\gamma}{\hbar c}\right)^{2\lambda+1} \times B(\sigma\lambda; J_i \rightarrow J_f) \times (1+\alpha), \quad (8)$$

with the electron conversion coefficient α, the multipolarity λ, the energy of the γ rays E_γ, and the radiation character σ. Since the decay between the states of the yrast band in even-even nuclei is dominated by $E2$ radiation, i.e., it is the only possible γ decay in the case of the $2_1^+ \rightarrow 0_{gs}^+$ transition, the $B(E2)$ values can be extracted from the determined mean lifetimes. Since a similar measurement method was used in Ref. [24] and the lifetimes are in good agreement with each other, weighted average values of the lifetimes of this work and [24] are given in Table I. The conversion coefficients for the determination of the $B(E2)$ values were taken from BrIccFO [40]. In the case of large uncertainties in $\tau_{weighted}$, asymmetric uncertainties are given for the $B(E2)$ values.

IV. DISCUSSION

A. Quadrupole collectivity

The new $B(E2)$ values do not show a saturation at midshell but a maximum shifted toward a lower neutron number, as can be seen in Fig. 8(a). Depicted are $B(E2; 2_1^+ \rightarrow 0_{gs}^+)$ strengths over the product N_pN_n [48] of numbers of proton valence particles or holes with respect to the major shell closures at $Z = 50$ and $Z = 82$ and of neutron valence particles or holes with respect to the major neutron shell closures at $N = 82$ and $N = 126$. The turning point of each graph for the different isotopic chains is at neutron midshell, since the number of valence particles (holes) maximize at midshell. Approaching midshell from lower neutron numbers, members of different isotopic chains show the same N_pN_n dependence as indicated by the dotted line in Fig. 8(a). Their collectivity, i.e., the $B(E2)$ strength, increases with the number of valence particles (holes) [48]. However, generally the $B(E2)$ strengths show an early drop before midshell is reached. In addition, an asymmetry is visible for the isotopic chains from Yb to W. That is, values past the inflection point are significantly lower,

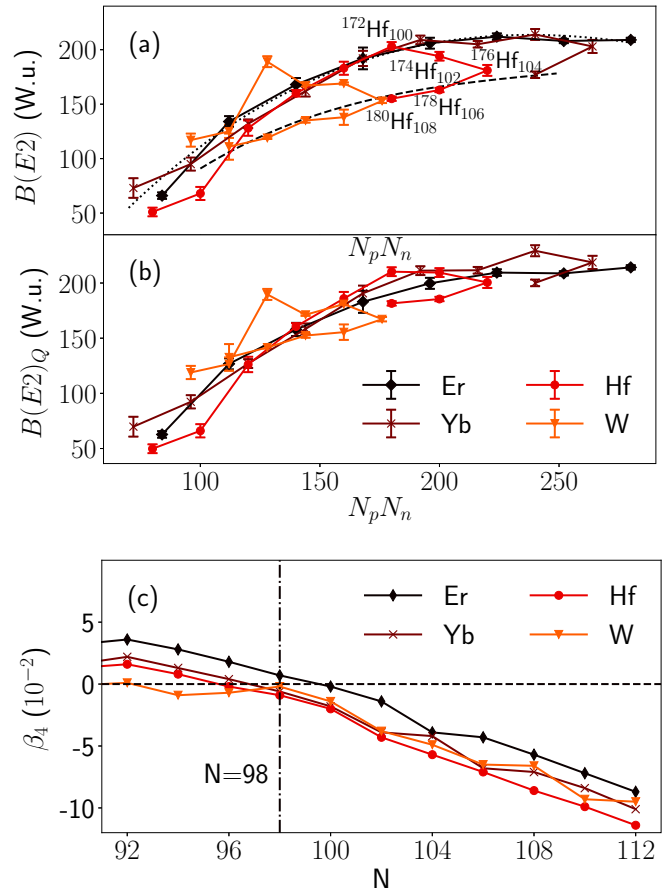

FIG. 8. (a) $B(E2; 2_1^+ \rightarrow 0_{gs}^+)$ strengths in W.u. plotted over the product proton valence particles (holes) and of neutron valence particles (holes) N_pN_n of the Er, Yb, Hf, and W isotopic chains. The gray dashed lines are plotted to guide the eyes. Data are taken from Refs. [1–14,24] and this work. (b) "Quadrupole" $B(E2)$ values, $B(E2)_Q$, vs. N_pN_n obtained by removing the β_4 hexadecapole deformations as described in Ref. [46]. β_2 values are taken from Ref. [28] and the β_4 values from Ref. [47]. (c) β_4 hexadecapole deformations vs. the neutron number. Data are taken from Ref. [47].

while again a continuous trend with respect to N_pN_n emerges [see the dashed line in Fig. 8(a)]. In the case of the Er isotopic chain, $B(E2)$ data are not available at and beyond midshell. The pre-mid-shell maximum of the $B(E2)$ strengths gets more pronounced for higher proton numbers. Zamfir *et al.* [46] proposed that the different trends of the $B(E2)$ values versus N_pN_n are due to the influence of the hexadecapole deformation parameter β_4 on the quadrupole moment Q. The expansion of the quadrupole moment shows the dependence of Q from β_4:

$$Q \propto \beta_2(1 + 0.36\beta_2 + 0.97\beta_4 + \dots). \quad (9)$$

The $B(E2)$ strength is proportional to Q^2 and therefore depends on β_4. The influence of β_4 can be removed by defining a "pure quadrupole" $B(E2)$ value [46]:

$$B(E2; 2_1^+ \rightarrow 0_{gs}^+)_Q = B(E2; 2_1^+ \rightarrow 0_{gs}^+) \left[\frac{Q(\beta_4 = 0)}{Q(\beta_4 \neq 0)}\right]^2. \quad (10)$$

The $B(E2)_Q$ values are shown in Fig. 8(b). The deformation parameters were taken from Ref. [28] or if not experimentally available from Ref. [47]. Note that β_4 changes slope from near-constant around $\beta_4 = 0$ to negative values at $N = 98$ in the Hf ($Z = 72$) isotopic chain [cf. Fig. 8(c)]. Figure 8(b) shows the effect of the hexadecapole correction: The $B(E2)$ values of the low-N branches of the curves increase while the values of the high-N branches decrease. That means athat the premature reversion of $B(E2)$ values is lifted. Although numerous indications for hexadeapole collectivity in the high-N, high-Z region of this major shell exist, a fully microscopic explanation of the early $B(E2)$ maximum has not been provided to date. Nevertheless, we examine the systematic behavior of another observable in the following, which has been discussed in conjunction with the evolution of collectivity, e.g., the energy ratios $R_{4/2}$ [49]. The average proton-neutron interaction of the last proton with the last neutron of the nucleus [48] is the double difference of binding energies, introduced by [50]:

$$\delta V_{pn}(Z,N) = \tfrac{1}{4}\{[BE(Z,N) - BE(Z,N-2)] - [BE(Z-2,N) - BE(Z-2,N-2)]\}, \quad (11)$$

with the binding energy $BE(Z,N)$. In general [51], δV_{pn} depends on the trend of the occupation of neutron and proton orbits from high j-low n to low j-high n orbits within a major shell. δV_{pn} is large for smaller values of δn and δj; hence, it should be large for regions where the overlap of neutron and proton orbits is large. Figure 9 shows the δV_{pn} obtained with the binding energies from Refs. [52,53] in an N-Z chart. δV_{pn} is in general small in the area above proton midshell and below neutron midshell and high in areas below neutron and proton midshell or above proton and neutron midshell. Figure 9(b) shows δV_{pn} of the Hf and W isotopic chains, calculated from available experimental data [52,53]. δV_{pn} is nearly constant before and after the neutron midshell but shows a sudden increase at $N = 104$. The increase is in accordance with the above-mentioned pattern. Potentially, the sudden increase of the δV_{pn} could already be reflected at $N < 104$ if neutrons already scatter early into the corresponding orbitals.

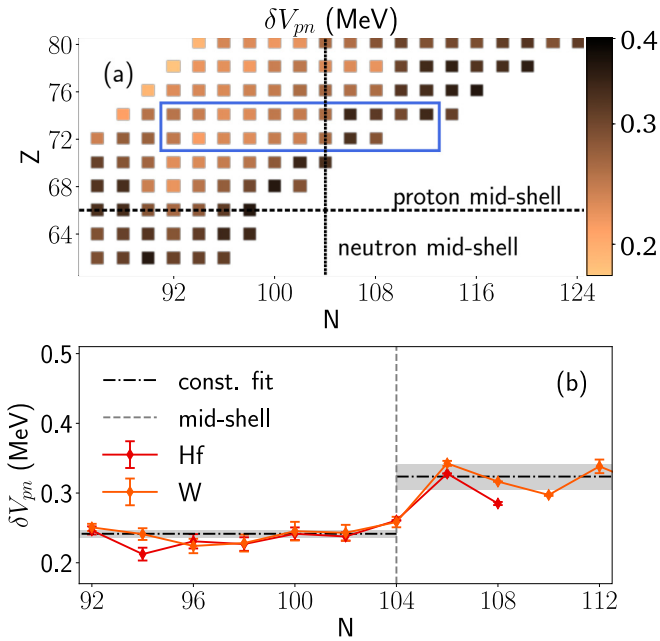

FIG. 9. (a) Depicted is the double difference δV_{pn} [20] in a N-Z chart. $N = 104$ is marked by the dotted dashed line. The areas marked in blue is shown in (b). The dotted dashed lines are fits with a constant to the Hf data before and after midshell, illustrating the sudden increase of δV_{pn} at $N = 104$ and the constant behavior before and after $N = 104$. The vertical gray dashed line marks the neutron midshell $N = 104$. Binding energies taken from Refs. [52,53].

Examining $E2$ observables within the ground-state bands of the Hf isotopes, first, we measured the $B(E2; 4_1^+ \rightarrow 2_1^+)$ value for the first time, although with large relative uncertainty. Nevertheless, the resulting value of the $B_{4/2}$ ratio fits well into the systematics shown in Fig. 10(b). All $B_{4/2}$ values of the Hf isotopes are distributed around the rotational limit of $B_{4/2,\mathrm{rot}} = 1.44$. Inspection of the $B(E2)$ rates of higher-lying states, however, as shown in Fig. 10(a), reveal significant and seemingly robust deviations from the rotational limit. In comparison to the rigid rotor value, the determined $B(E2; 6_1^+ \rightarrow 4_1^+)$ transition strength of ^{174}Hf is unexpectedly smaller than the corresponding $B(E2; 4_1^+ \rightarrow 2_1^+)$ value. For the case of ^{176}Hf a similar trend cannot be excluded, because of the large

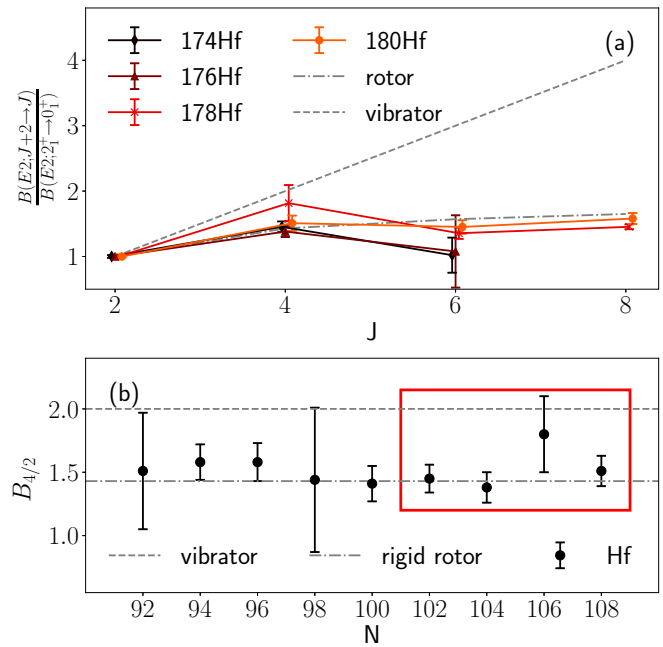

FIG. 10. (a) Normalized $B(E2; J \rightarrow J-2)$ transition strengths are plotted over J for the isotopes ^{174,176,178,180}Hf. ^{178,180}Hf are close to the rigid rotor limit. The $B(E2; 6_1^+ \rightarrow 4_1^+)$ strength is significantly lower than the $B(E2; 4_1^+ \rightarrow 2_1^+)$ strength of ^{174}Hf. The isotopes are slightly shifted for a better visibility. (b) Ratio $B_{4/2}$ of the $B(E2)$-transition strengths $B(E2; 4_1^+ \rightarrow 2_1^+)$ and $B(E2; 2_1^+ \rightarrow 0_{gs}^+)$. Shown in the red box are the averaged values from this work and Refs. [12,13,24] and outside the box the known literature data taken from Refs. [5–9]. The dotted line represents the value obtained in the rigid rotor limit and in the vibrator limit.

TABLE II. The $B(E\lambda)$ strengths of ^{176}Hf were determined with the known branching ratios taken from Ref. [11], the conversion coefficients taken from Ref. [40], and the multipole-mixing ratios of the $2_1^- \rightarrow 2_1^+$ transition taken from Ref. [43].

	$B(M/E\lambda)$ in $\mu_N^2 b^{2\lambda-2}/e^2 b^\lambda$	$B(E\lambda)$ (W.u.)
$B(E1; 2_1^- \rightarrow 2_1^+)$	$4(2) \times 10^{-10}$	$2(1) \times 10^{-8}$
$B(M2; 2_1^- \rightarrow 2_1^+)$	$10(3) \times 10^{-3}$	$2(1) \times 10^{-2}$
$B(E3; 2_1^- \rightarrow 2_1^+)$	$6(2) \times 10^{-2}$	30(12)
$B(E1; 3_1^- \rightarrow 4_1^+)$	$8^{+6}_{-3} \times 10^{-8}$	$4^{+3}_{-2} \times 10^{-6}$
$B(E1; 3_1^- \rightarrow 2_1^+)$	$9^{+9}_{-3} \times 10^{-8}$	$4^{+5}_{-1} \times 10^{-6}$

uncertainty of the $B(E2; 6_1^+ \rightarrow 4_1^+)$ value. Unfortunately, no data are available for the higher-lying states of the yrast band of these two isotopes. Similar results were obtained in Ref. [24] and in other rare-earth isotopes, e.g., ^{162}Yb [54] and a too-low, with respect to the rigid rotor limit, $B(E2; 6_1^+ \rightarrow 4_1^+)$ value seems to be a reoccurring and so far unexplained feature in the rare-earth region, while other $B(E2)$ values, e.g., in ^{178,180}Hf, are in good agreement with the rigid-rotor limit. Therefore, again, a change in rotational structure past $N = 100$ is seen in the Hf isotopes.

B. $K^\pi = 2^-$ band of ^{176}Hf

In ^{176}Hf, in addition, the low-lying negative-parity band was observed. The 2_1^- and 3_1^- states have been assigned as members of a $K^\pi = 2^-$ band in Refs. [41,42]. The expected $E1$ decay transitions from this band to the yrast band are first forbidden transitions ($\Delta K = 2$) according to the Alaga rules [55] and from conversion-electron data a large admixture of $M2$ and $E3$ has been confirmed for the decay transitions of the 2_1^- state [41]. The decay transitions of the 3_1^- state were assigned to have $E1$ character. Unfortunately, the decay of the 3_1^- state to the 2_1^- state at 65 keV was not observed or is obscured by x-ray transitions. The 3_1^- state is short lived with a mean lifetime of $\tau(3_1^-) = 25(12)$ ps. The extracted mean lifetime of the 2_1^- state is slightly below the adopted literature value [11] but in good agreement with other measurements [43].

Under the assumption that the transition width of the transition $3_1^- \rightarrow 2_1^-$ is negligible, an upper limit for the $E1$ transition strength of the two other decay transitions of the 3_1^- state can be determined. Even from this upper limit the suppression of the transition rates is visible. The $E1$ strength is three orders of magnitude smaller than other $E1$ strength in this nucleus. An overview over the $E1$ strength distribution in ^{176}Hf was given in Ref. [56]. From the new weighted average value of $\tau(2_1^-)$ the transition strengths of its decay $2_1^- \rightarrow 2_1^+$ can be determined with the known multipole mixing ratios from Ref. [43] and the branching ratios from Ref. [11]. The transition strengths are given in Table II.

V. SUMMARY

In this work several lifetimes of yrast states of the hafnium isotopes with $A = 174$, 176, 178, and 180 have been determined using fast-electronic scintillation timing and a Coulomb-excitation analysis. The mean lifetimes of the 2_1^+ and 4_1^+ states of all isotopes and the lifetimes of the 6_1^+ states of ^{174,178,180}Hf have been measured and are in good agreement with other recent results [24]. The mean lifetime, $\tau(4_1^+) = 85(13)$ ps, of ^{178}Hf has been determined for the first time. From these lifetimes the $B(E2)$ transition strengths between the yrast states have been calculated and the $B_{4/2}$ ratios have been extracted.

In addition, the mean lifetimes of the 2_1^- and the 3_1^- states of ^{176}Hf have been determined.

ACKNOWLEDGMENTS

The authors thank the tandem accelerator crew for their support during the experiment. This work was supported by the Deutsche Forschungsgemeinschaft, under Grants No. SFB 1245 and No. JO 391/16-2; the BMBF under Grant No. 05P15RDFN1 within the collaboration 05P15 NuSTAR R&D and Grants No. 05P15RDFN9 and No. 05P18RDFN9; and by the U.S. DOE under Grant No. DE-FG02-91ER40609. This work was partially supported by the UK Science and Technologies Facilities Council (STFC) via Grants No. ST\L0057\1 and No. ST\P005314\1. P.H.R. acknowledges partial support from the UK Department of Business, Energy and Industrial Strategy (BEIS) via the National Measurement System (NMS).

[1] C. W. Reich, Nucl. Data Sheets **113**, 2537 (2012).
[2] N. Nica, Nucl. Data Sheets **141**, 1 (2017).
[3] C. W. Reich, Nucl. Data Sheets **105**, 557 (2005).
[4] C. W. Reich, Nucl. Data Sheets **108**, 1807 (2007).
[5] B. Singh and J. Chen, Nucl. Data Sheets **147**, 1 (2018).
[6] C. M. Baglin, Nucl. Data Sheets **109**, 1103 (2008).
[7] C. M. Baglin, Nucl. Data Sheets **111**, 1807 (2010).
[8] C. M. Baglin, Nucl. Data Sheets **96**, 611 (2002).
[9] B. Singh, Nucl. Data Sheets **75**, 199 (1995).
[10] E. Browne and H. Junde, Nucl. Data Sheets **87**, 15 (1999).
[11] M. S. Basunia, Nucl. Data Sheets **107**, 791 (2006).
[12] E. Achterberg, O. A. Capurro, and G. V. Marti, Nucl. Data Sheets **110**, 1473 (2009).
[13] E. A. McCutchan, Nucl. Data Sheets **126**, 151 (2015).
[14] B. Singh, Nucl. Data Sheets **130**, 21 (2015).
[15] F. Iachello and A. Arima, *The Interacting Boson Model* (Cambridge University Press, Cambridge, 2006).
[16] V. Werner, N. Cooper, J.-M. Régis, M. Rudigier, E. Williams, J. Jolie, R. B. Cakirli, R. F. Casten, T. Ahn, V. Anagnostatou, Z. Berant, M. Bonett-Matiz, M. Elvers, A. Heinz, G. Ilie, D. Radeck, D. Savran, and M. K. Smith, Phys. Rev. C **93**, 034323 (2016).

[17] J. Y. Zhang, R. F. Casten, A. Wolf, Z. Berant, R. B. Cakirli, N. V. Zamfir, and E. A. McCutchan, Phys. Rev. C **73**, 037301 (2006).

[18] Z. Berant, A. Wolf, N. V. Zamfir, M. A. Caprio, D. S. Brenner, N. Pietralla, R. L. Gill, R. F. Casten, C. W. Beausang, R. Krucken, C. J. Barton, J. R. Cooper, A. A. Hecht, D. M. Johnson, J. R. Novak, H. Cheng, B. F. Albanna, and G. Gurdal, Phys. Rev. C **69**, 034320 (2004).

[19] B. A. Bian, Y.-M. Di, G.-L. Long, Y. Sun, J. Y. Zhang, and J. A. Sheikh, Phys. Rev. C **75**, 014312 (2007).

[20] R. B. Cakirli, K. Blaum, and R. F. Casten, Phys. Rev. C **82**, 061304 (2010).

[21] A. Costin, T. Ahn, B. Bochev, K. Dusling, T. C. Li, N. Pietralla, G. Rainovski, and W. Rother, Phys. Rev. C **74**, 067301 (2006).

[22] J.-M. Régis, T. Materna, S. Christen, C. Bernards, N. Braun, G. Breuer, C. Fransen, S. Heinze, J. Jolie, T. Meersschaut, G. Pascovici, M. Rudigier, L. Steinert, S. Thiel, N. Warr, and K. O. Zell, Nucl. Instrum. Methods Phys. Res., Sect. A **606**, 466 (2009).

[23] M. Rudigier, J.-M. Régis, J. Jolie, K. O. Zell, and C. Fransen, Nucl. Phys. A **847**, 89 (2010).

[24] M. Rudigier, K. Nomura, M. Dannhoff, R.-B. Gerst, J. Jolie, N. Saed-Samii, S. Stegemann, J.-M. Régis, L. M. Robledo, R. Rodríguez-Guzmán, A. Blazhev, C. Fransen, N. Warr, and K. O. Zell, Phys. Rev. C **91**, 044301 (2015).

[25] K. Kumar, Phys. Rev. Lett. **28**, 249 (1972).

[26] D. Cline, Annu. Rev. Nucl. Part. Sci. **36**, 683 (1986).

[27] V. Werner, P. von Brentano, and R. V. Jolos, Phys. Lett. B **521**, 146 (2001).

[28] B. Pritychenko, M. Birch, B. Singh, and M. Horoi, At. Data. Nucl. Data Tables **107**, 1 (2016).

[29] D. Cline, Bull. Am. Phys. Soc. **14**, 726 (1969).

[30] D. Bucurescu, I. Căta-Danil, G. Ciocan, C. Costache, D. Deleanu, R. Dima, D. Filipescu, N. Florea, D. G. Ghiţă, T. Glodariu, M. Ivaşcu, R. Lică, N. Mărginean, R. Mărginean, C. Mihai, A. Negret, C. R. Niţă, A. Olăcel, S. Pascu, T. Sava, L. Stroe, A. Şerban, R. Şuvăilă, S. Toma, N. V. Zamfir, G. Căta-Danil, I. Gheorghe, I. O. Mitu, G. Suliman, C. A. Ur, T. Braunroth, A. Dewald, C. Fransen, A. M. Bruce, Z. Podolyák, P. H. Regan, and O. J. Roberts, Nucl. Instrum. Methods Phys. Res., Sect. A **837**, 1 (2016).

[31] H. Mach, R. L. Gill, and M. Moszyński, Nucl. Instrum. Methods A **280**, 49 (1989).

[32] M. Moszyński and H. Mach, Nucl. Instrum. Methods A **277**, 407 (1989).

[33] J.-M. Régis, H. Mach, G. S. Simpson, J. Jolie, G. Pascovici, N. Saed-Samii, N. Warr, A. Bruce, J. Degenkolb, L. M. Fraile, C. Fransen, D. G. Ghita, S. Kisyov, U. Koester, A. Korgul, S. Lalkovski, N. Mărginean, P. Mutti, B. Olaizola, Z. Podolyak, P. H. Regan, O. J. Roberts, M. Rudigier, L. Stroe, W. Urban, and D. Wilmsen, Nucl. Instrum. Methods A **726**, 191 (2013).

[34] N. Mărginean, D. L. Balabanski, D. Bucurescu, S. Lalkovski, L. Atanasova, G. Căta-Danil, I. Căta-Danil, J. M. Daugas, D. Deleanu, P. Detistov, G. Deyanova, D. Filipescu, G. Georgiev, D. Ghiţă, K. A. Gladnishki, R. Lozeva, T. Glodariu, M. Ivaşcu, S. Kisyov, C. Mihai, R. Mărginean, A. Negret, S. Pascu, D. Radulov, T. Sava, L. Stroe, G. Suliman, and N. V. Zamfir, Euro. Phys. J. A **46**, 329 (2010).

[35] J. Wiederhold, R. Kern, C. Lizarazo, N. Pietralla, V. Werner, R. V. Jolos, D. Bucurescu, N. Florea, D. Ghita, T. Glodariu, R. Lica, N. Marginean, R. Marginean, C. Mihai, R. Mihai, I. O. Mitu, A. Negret, C. Nita, A. Olacel, S. Pascu, L. Stroe, S. Toma, and A. Turturica, Phys. Rev. C **94**, 044302 (2016).

[36] L. Boström, B. Olsen, W. Schneider, and E. Matthias, Nucl. Instrum. Methods. **44**, 61 (1966).

[37] Z. Bay, Phys. Rev. **77**, 419 (1950).

[38] J.-M. Régis, G. Pascovici, J. Jolie, and M. Rudigier, Nucl. Instrum. Methods A **622**, 83 (2010).

[39] M. T. Gillin and N. F. Peek, Phys. Rev. C **4**, 1334 (1971).

[40] T. Kibédi, T. W. Burrows, M. B. Trzhaskovskaya, P. M. Davidson, and C. W. Nestor, Nucl. Instrum. Methods A **589**, 202 (2008).

[41] F. M. Bernthal, J. O. Rasmussen, and J. M. Hollander, Phys. Rev. C **3**, 1294 (1971).

[42] T. L. Khoo, J. C. Waddington, Z. Preibisz, and M. W. Johns, Nucl. Phys. A **202**, 289 (1973).

[43] K. E. G. Löbner, H. A. Smith, and M. E. Bunker, Nucl. Phys. A **179**, 276 (1972).

[44] H. Ower, Dissertation, Johann Wolfgang Goethe-Universität, Frankfurt am Main, 1980.

[45] A. Winther and J. De Boer, *A Computer Program for Multiple Coulomb Excitation* (Academic Press, New York, 1966).

[46] N. V. Zamfir, G. Hering, R. F. Casten, and P. Paul, Phys. Lett. B **357**, 515 (1995).

[47] P. Möller, A. J. Sierk, T. Ichikawa, and H. Sagawa, At. Data. Nucl. Data Tables **109-110**, 1 (2016).

[48] R. F. Casten and N. V. Zamfir, J. Phys. G **22**, 1521 (1996).

[49] R. B. Cakirli and R. F. Casten, Phys. Rev. Lett. **96**, 132501 (2006).

[50] J.-Y. Zhang, R. F. Casten, and D. S. Brenner, Phys. Lett. B **227**, 1 (1989).

[51] R. B. Cakirli, D. S. Brenner, R. F. Casten, and E. A. Millman, Phys. Rev. Lett. **94**, 092501 (2005).

[52] W. J. Huang, G. Audi, M. Wang, F. G. Kondev, S. Naimi, and X. Xu, Chin. Phys. C **41**, 030002 (2017).

[53] M. Wang, A. G., F. G. Kondev, W. J. Huang, S. Naimi, and X. Xu, Chin. Phys. C **41**, 030003 (2017).

[54] E. A. McCutchan, N. V. Zamfir, R. F. Casten, H. Ai, H. Amro, M. Babilon, D. S. Brenner, G. Gürdal, A. Heinz, R. O. Hughes, D. A. Meyer, C. Plettner, J. Qian, J. J. Ressler, N. J. Thomas, V. Werner, E. Williams, and R. Winkler, Phys. Rev. C **73**, 034303 (2006).

[55] G. Alaga, K. Alder, A. Bohr, and B. R. Mottelson, Dan. Mat. Fys. Medd. **29**, 1 (1955).

[56] M. Scheck, D. Belic, P. von Brentano, J. J. Carroll, C. Fransen, A. Gade, H. von Garrel, U. Kneissl, C. Kohstall, A. Linnemann, N. Pietralla, H. H. Pitz, F. Stedile, R. Toman, and V. Werner, Phys. Rev. C **67**, 064313 (2003).